Role of the Direct Reaction $H_2S + SO_2$ in the Homogeneous Claus Reaction

Karina Sendt* and Brian S. Haynes

Department of Chemical Engineering, University of Sydney, NSW 2006, Australia

Received: May 18, 2005; In Final Form: July 14, 2005

Quantum chemical methods at the Gaussian-2 and -3 levels of theory have been used to investigate the reactions between H_2S, SO_2, and S_2O such as might occur in the front-end furnace of the Claus process. The direct reaction between H_2S and SO_2 occurs via a 5-centered transition state with an initial barrier of ∼135 kJ mol^{-1} and an overall barrier of ∼153 kJ mol^{-1} to produce S_2O and H_2O. We indicate approximate values here because there are a number of isomers in the reaction pathway that have barriers slightly different from those quoted. The presence of a water molecule lowers this by ∼60 kJ mol^{-1}, but the van der Waals complex required for catalysis by water is thermodynamically unfavorable under the conditions in the Claus reactor. The direct reaction between H_2S and S_2O can occur via two possible pathways; the analogous reaction to $H_2S + SO_2$ has an initial barrier of ∼117 kJ mol^{-1} and an overall barrier of ∼126 kJ mol^{-1} producing S_3 and H_2O, and a pathway with a 6-centred transition state has a barrier of ∼111 kJ mol^{-1}, producing HSSSOH. Rate constants, including a QRRK analysis of intermediate stabilization, are reported for the kinetic scheme proposed here.

1. Introduction

The Claus process is employed to convert waste H_2S from many industrial processes to elemental sulfur. In the modern "modified" process, some of the H_2S is converted to SO_2 by combustion in a furnace; the H_2S and SO_2 are then reacted in a series of catalyst beds with liquid sulfur removal in intervening condensers. The two steps of the overall process may be represented as

$$H_2S + {}^3/_2O_2 \rightarrow SO_2 + H_2O$$

$$2H_2S + SO_2 \rightarrow {}^3/_2S_2 + 2H_2O$$

In practice, the front-end furnace in which H_2S is oxidized to SO_2 also sees significant homogeneous reaction between H_2S and SO_2, to the extent that the design of this furnace and of the ensuing catalytic reactors is significantly impacted. It is the kinetics of this homogeneous process, and its catalysis by H_2O, that we report on here.

Though kinetic models for H_2S oxidation[1−3] and more recently H_2S thermolysis[4] are available, the only theoretical work on the reaction between H_2S and SO_2 has been the identification of possible intermediates by Steudel and co-workers.[5,6] They identified a number of stable H/S/O species and predicted thiosulfurous acid HSS(O)OH to be the most stable product from the addition of H_2S to SO_2. They also postulated[6] that water acts as a hydrogen donor/acceptor after the formation of a stable $H_2S{\cdot}SO_2{\cdot}H_2O$ complex and hence the reaction in practice may be influenced by the stability of a range of van der Waals complexes. Finally, Drozdova and Steudel[6] have pointed out the role of these reactions in the aqueous Wackenroder reaction (which produces a variety of sulfurous oxyacids from reaction of H_2S with SO_2 in solution).

In this study we employ quantum chemical methods to examine the kinetics of the reaction between H_2S and SO_2 to form HSS(O)OH. We also study the molecular rearrangement of HSS(O)OH to form S_2O and H_2O. Both reactions are studied for dry conditions (on the $H_2S_2O_2$ potential energy surface) and for catalysis by H_2O ($H_4S_2O_3$ surface). The analogous reaction between H_2S and S_2O is also characterized as a possible means for decomposing S_2O at low concentrations formed from the homogeneous Claus process (H_2S_3O surface). A low-barrier decomposition reaction between two S_2O molecules has been recently proposed[7] to explain the instability of S_2O at pressures above 1 mbar; however, no kinetics were included.

2. Computational Method

Quantum chemical calculations were carried out on all molecules at the G2[8] and G3[9] levels of theory. For the most part, these procedures were carried out as usual, but in selected cases the methods for determining the geometry were altered. In the case of the van der Waals complexes VdW1-4, the geometries were optimized at the MP2(full)/6-31++G(d,p) level of theory. Diffuse functions were included in this geometry optimization to account for weak intermolecular bonds. The resulting MP2 frequencies were scaled by 0.9427 when included in the G2 and G3 theories, rather than 0.8929, which is customary for SCF values. As the authors are not aware of any recommended scaling factor for frequencies using this particular basis set, the scaling factor was taken from the optimized MP2=full/6-31G(d) value as suggested in ref 10, where the choice of basis set was shown to have little effect on the scaling factor. The relative energies of rotamers were calculated using the Gaussian methods with the MP2=full/6-31G(d) optimized geometries and scaled frequencies. To describe more accurately transition states involving the breaking and formation of covalent bonds, CASSCF/6-31G(d) optimizations with six active electrons in six active orbitals were performed. Here, the frequency scaling factor was chosen to be identical to the corresponding SCF value (i.e., 0.8929). When the nature of the transition state was not unambiguous, the intrinsic reaction coordinate was followed to determine reactants and products. The Gaussian-3

* Corresponding author. E-mail: ksendt@chem.eng.usyd.edu.au.

10.1021/jp052622i CCC: $30.25
Published on Web 08/19/2005

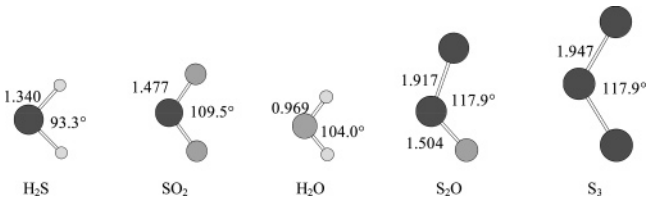

Figure 1. Molecular geometries for reactant and product species. Bond lengths in Å.

method is reported to have an estimated error of ±4 kJ mol^{-1} for heats of formation of stable species; for the transition states here we estimate an error in the vicinity of 15 kJ mol^{-1} due to the T_1 diagnostics being slightly greater than 0.02. It is worth noting that although there are large errors in the computed heats of formation for sulfur oxide species based on atomization energies (e.g., 20 kJ mol^{-1} for SO_2 at the G3 level[9]), the relative energies should be in good agreement with experiment, as the bonding patterns are similar. The Gaussian-2 results are also reported here for comparison of previous studies.[4,11]

In addition to the Gaussian methods (which ideally would minimize basis set superposition error), a large basis set method (LBS) with full counterpoise correction[12] was made for some of the van der Waals complexes. The MP2(full)/6-311++G(d,p) geometries and vibrational frequencies (scaled by 0.9427) were used. This was carried out using the CCSD(T) method with the 6-311++G(d,p) basis set.

The electronic structure calculations were performed with Gaussian 98[13] with the exception of the CASSCF calculations which were performed using Dalton.[14]

The energies and thermodynamic properties were extrapolated to nonzero temperatures using the standard formulas,[15] and the high-pressure rate constants were calculated using transition state theory.[16] In this treatment, hindered rotations were treated as vibrations. Where a number of rotamers exist for an intermediate, the contribution to the partition function was based on the relative energy above the most stable rotamer. Optical isomerism in transition states and intermediates was accounted for by including a factor of 2 in the relevant partition functions. Tunneling corrections were estimated according to Wigner's formulation.[17] These corrections are typically of order 3−5 at 300 K, reducing to ∼1.1 at 2000 K. Comparison to accurate quantal calculations in collinear systems have shown that the Wigner correction has an accuracy of ∼15% at 300 K and ∼60% at 1500 K.[18]

The corrected rate constants were then fitted to a three-parameter Arrhenius form using a least-squares method.

To understand the behavior of the $H_2S_2O_2$ and H_2S_3O systems at lower pressures, the QRRK method[19] was used to treat the intermediates as chemically activated species.

3. Results and Discussion

3.1. Quantum Chemical Results. Geometrical parameters for the small reactant and product species are presented in Figure 1. Figures 2 and 3 contain the geometries and reaction schematics for species on the $H_2S_2O_2$ surface, with relative energies in Table 1. Figures 4 and 5 and Table 2 contain the corresponding parameters for the $H_4S_2O_3$ surface, and Figures 6 and 7 and Table 3 contain the results for the H_2S_3O surface. The computed kinetic and thermodynamic parameters are reported in Tables 4 and 5, respectively. Complete structures and vibrational frequencies for all species are contained in Table 1S.

$H_2S_2O_2$ Surface. In this reaction, hydrogen sulfide and sulfur dioxide combine to form thiosulfurous acid HSS(O)OH (I) and subsequently S_2O and H_2O in a two-step process as shown in Figure 3. Although a weak van der Waals complex between H_2S and SO_2 exists, it is unlikely to be stable at the temperatures considered in this study, as discussed later. The barrier for the first step was found to be around 135 ± 15 kJ mol^{-1}, indicating that this process is only feasible at high temperatures. Two possible transition states were found corresponding to a cis (TS1a) and trans (TS1b) configuration, each with two possible optical isomers. Both transition states were found to have similar geometric properties to the reaction between H_2O and SO_2 to form H_2SO_3.[11,20]

Thiosulfurous acid (I), was reported to be the most stable isomer of $H_2S_2O_2$, on the basis of MP2 calculations, albeit by a small amount.[6] However, the energy of (I) (Table 1) is predicted by the Gaussian methods to be ∼50 kJ mol^{-1} lower in energy than found previously at the MP2 level.[6] This difference is due to the higher level of both basis set and theory used in the present G2 and G3 calculations: 20 kJ mol^{-1} of this difference may be ascribed to the extension of the level of theory to QCISD(T), and the remaining 30 kJ mol^{-1} is due to the inclusion of extra polarization functions. It is not clear whether the prediction[5] that (I) is the lowest energy isomer on the $H_2S_2O_2$ potential energy surface would hold at the G2 and G3 levels of theory, but this was not examined here as (I) involves the least amount of molecular rearrangement from H_2S+SO_2.

Rotation about the SS and SO bonds in (I) gives rise to a number of rotamers a−f, as shown in Figure 2. Conversion between the various rotamers is facile, with the barrier to rotation between Ia and Ib just 10 kJ mol^{-1}.

Intermediate (I) is able to undergo hydrogen transfer as in TS1, with concomitant bond cleavage to form S_2O and H_2O. The barrier for this step (TS2) was found to be ∼120 kJ mol^{-1} above (I). Again, two possible transition states were located TS2a (cis) and TS2b (trans). The overall reaction $H_2S + SO_2 \rightarrow H_2O + SO_2$ was found to be 17 kJ mol^{-1} endothermic, in good agreement with the experimental value of 19 kJ mol^{-1}, and considerably less than the MP2 result.[6] For all species there was good agreement between G2 and G3 results and experimental literature values where reported.

Given the relative heights of the barriers for TS1 and TS2, and the fact that the intermediate (I) was found to be in a deep well, a kinetic analysis treating (I) as a chemically activated intermediate is appropriate. The QRRK methodology[19] was used in which the chemically activated (I) could return to $H_2S + SO_2$, react to form $H_2O + S_2O$, or stabilize as (I). Transition state theory was used to obtain the required high-pressure rate constants, with each process the sum over the two possible transition states. All rotamers of (I) contributed to the partition function according to the relative energy of each rotamer:

$$Q_{\text{rotamer}} = \sum_i e^{-\Delta E_i/RT}$$

Additionally, a factor of 2 was included in the partition functions of TS1a, TS1b, (I), TS2a and TS2b to account for optical isomerism. The stabilization rate was computed in 1 atm of N_2, with the Lennard-Jones parameter ϵ for (I) chosen to put its boiling point at 470 K, 30 K higher than that of H_2S_3. The energy dependence of the density of states, F_E, was chosen to be 1.1, similar to that suggested in ref 19 and used previously.[4] Under the most sensitive conditions (the highest temperature), varying F_E from 0.8 to 1.5 resulted in a change of just of 30% in the stabilization rate.

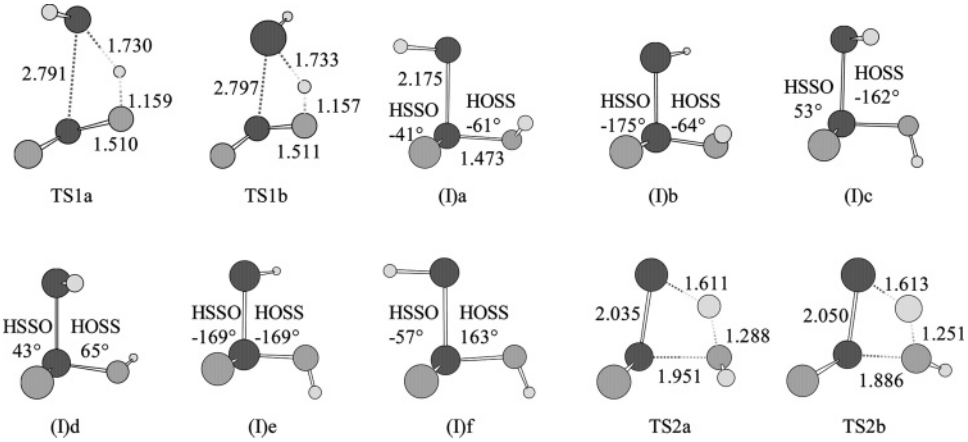

Figure 2. Molecular geometries of the species on the $H_2S_2O_2$ potential energy surfaces. Bond lengths in Å.

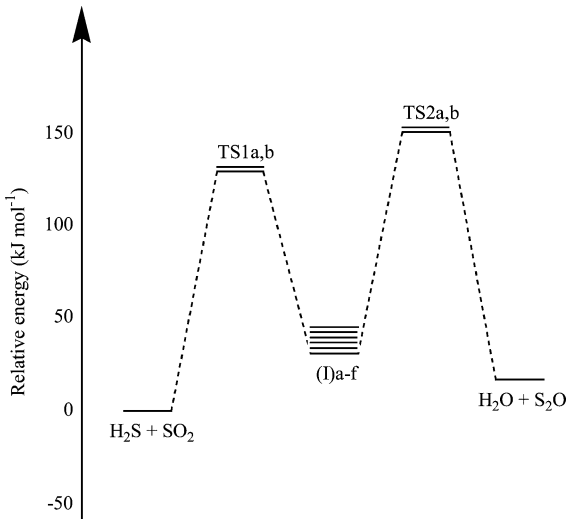

Figure 3. Potential energy surface for the reaction between H_2S and SO_2.

TABLE 1: Relative Energies of Species on the $H_2S_2O_2$ Potential Energy Surface

	relative energy (kJ mol-1)		
species	G2	G3	lit. values
$H_2S + SO_2$	0	0	
TS1a	136[a]	131[a]	
TS1b	138[a]	132[a]	
(I)a	30	29	81.3[b]
(I)b	31[c]	30[c]	
(I)c	42[c]	41[c]	
(I)d	43[c]	42[c]	
(I)e	43[c]	42[c]	
(I)f	39[c]	44[c]	
TS2a	151[a]	150[a]	
TS2b	155[a]	155[a]	
$S_2O + H_2O$	16	17	38.1,[b] 19.1[d]

[a] CASSCF(6,6)/6-31G(*d*) optimized geometry. [b] MP2/6-311G(d,p) values calculated from ref 6. [c] Energies relative to (I)a calculated at G2 or G3 level with MP2/6-31G(*d*) frequencies. [d] 298 K values calculated from $\Delta H^0_{f,298}$ from NIST webbook.[26]

At all temperatures the rate for thiosulfurous acid returning to reactants ($H_2S + SO_2$) was considerably higher than the rate for forming products ($H_2O + S_2O$). Thus, the QRRK calculations in 1 atm N_2 showed that even at 2000 K, only 5.5% of reaction flux over TS1 continued over TS2 to form $S_2O + H_2O$. At 300 K, >99% of reaction flux over TS1 is stabilized as (I), and this decreases with temperature to ~2% at 2000 K. Varying the pressure of the bath gas indicates that the stabilization reaction is at the high-pressure limit at 300 K, whereas it is near the low-pressure limit at 2000 K: in 0.1 atm N_2, ~0.25% of reaction flux is stabilized as (I), whereas in 10 atm N_2, ~12% is stabilized. Secondary reactions of (I) are beyond the scope of this paper, however it is conceivable that low-barrier bimolecular reactions with species such as SH and O_2 (which are present in the homogeneous Claus process) would be competitive with the reverse process returning to reactants. In this situation, the disappearance of reactants would be described by the sum of R1 and R2 in Table 4. The computed QRRK rate constants for the processes $H_2S + SO_2 \rightarrow$ (I) and $H_2S + SO_2 \rightarrow H_2O$ and S_2O are presented in Table 4.

$H_4S_2O_3$ Surface. It has been long known[6] that the reaction between H_2S and SO_2 is catalyzed by the presence of water. Previous work on the hydrolysis of SO_2[11,20] has shown that water molecules, by virtue of being able to both accept and donate hydrogen atoms, could lower the barriers to reaction if stable van der Waals complexes could be formed. The van der Waals complexes between H_2S, H_2O, and SO_2 were studied to determine the most likely complex(es) to form. Calculations at the G2 and G3 level of theories indicated that the stability of complexes decreased as $H_2O{\cdot}SO_2$ (VdW1) $\gg$ $H_2O{\cdot}H_2S$ (VdW2) > $H_2S{\cdot}SO_2$ (VdW3). It is considered most unlikely that either the VdW2 or VdW3 complexes would exist for an appreciable length of time under reaction conditions of interest. Further investigation of the VdW1 complex as well as that of the $H_2S{\cdot}H_2O{\cdot}SO_2$ (VdW4) complex was carried out to determine the likelihood of their playing an important role under the conditions of the Claus process. Their energetics were studied with the CCSD(T)/6-311++G(d,p) method using a full counterpoise correction to compensate for basis set superposition error. The VdW1 complex had been studied previously using the Gaussian-2 method[11] and the QCISD(T)/6-311++G(d,p)//MP2/6-31G(d) level,[20] as reported in Table 2. The results obtained in this study are similar in range to the previously reported values, with our G2 and G3 results in this study predicting the complex to be more stable than earlier values[11] due to the different method of geometry optimization used here. The CCSD(T)/6-311++G(d,p) energies with full counterpoise correction are at the lower end of the energy range as predicted by ref 20. Thus, the VdW1 complex is predicted to be stable by 10−19 kJ mol^{-1}.

The VdW1 complex may react further with H_2O,[11] or with H_2S to form the VdW4 complex. The ratio of these pathways will depend on prevailing conditions. The addition of H_2S is predicted to be stable by 4−10 kJ mol^{-1} (Table 2), again with the Gaussian methods predicting greater stability than the

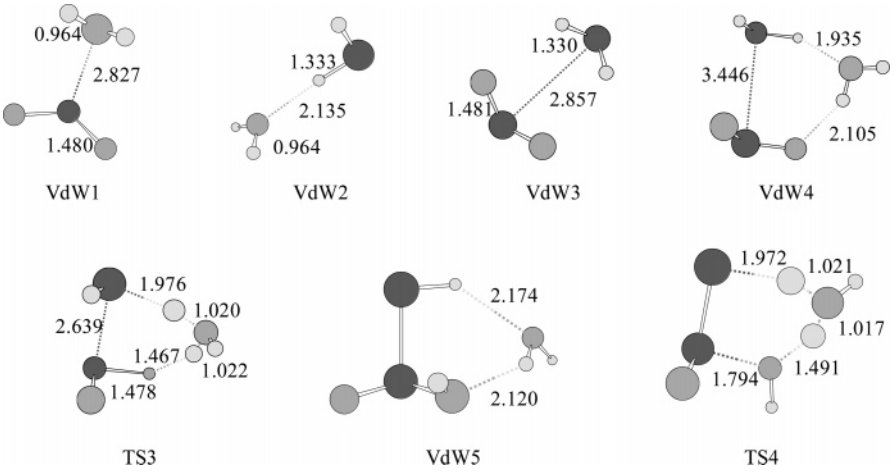

Figure 4. Molecular geometries of the species on the $H_4S_2O_3$ potential energy surfaces. Bond lengths in Å.

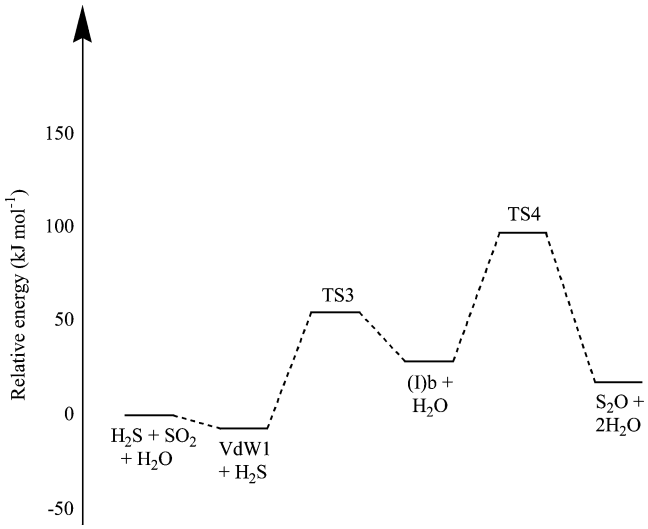

Figure 5. Potential energy surface for the reaction between H_2S, SO_2, and H_2O for pathways included in reaction scheme.

TABLE 2: Relative Energies of the Species on the $H_4S_2O_3$ Potential Energy Surface

	relative energies (kJ mol^{-1})			
species	G2	G3	LBS[a]	lit. values
$H_2S + SO_2 + H_2O$	0	0	0	
H_2S + VdW1	−17[b]	−19[b]	−10	−7.6,[c] −14.6[d]
SO_2 + VdW2	−6[b]	−6[b]		
H_2O + VdW3	−7[b]	−8[b]		
VdW4	−27[b]	−29[b]	−14	
TS3	62[e]	54[e]		
(I)b + H_2O	31	30		
VdW5	14[b]	12[b]	18[f]	
TS4	103[e]	98[e]		
$S_2O + 2H_2O$	16	17		

[a] CCSD(T)/6-311++G(d,p)//MP2(full)/6-31++G(d,p) with counterpoise correction. [b] MP2(full)/6-31++G(d,p) optimized geometry and frequencies. [c] QCISD(T)/6-311++G(d,p)//MP2/6-31+G(d,p) with counterpoise correction from ref 19. [d] G2 value from ref 20. [e] CASSCF(6,6)/6-31G(*d*) optimized geometry. [f] Based on the G3 energy for (I)b.

CCSD(T) with full counterpoise correction. The computed heat of formation reported in Table 5 is based on the result obtained using CCSD(T) with full counterpoise correction. As can be clearly seen from Figure 4, the VdW1 complex must rearrange geometrically to allow the H_2S molecule to add to it but the energy required for this rearrangement was found to be below the energy required to break it apart into its constituent molecules. By way of comparison, it is observed that no such rearrangement is needed for the addition of a second water molecule in the hydrolysis of SO_2 (i.e., for VdW1 + H_2O) and the complex that results in that case is 30 kJ mol^{-1} stable at the G2 level of theory.[11]

The VdW4 complex can undergo molecular rearrangement to form the intermediate HSS(O)OH and water. Although a number of configurations exist for the transition state TS3, only one was studied here to understand the size of the catalytic effect of water. The process involves a barrier of 70−87 kJ mol^{-1}, depending on the method used to describe the VdW4 complex. This barrier is approximately 45 kJ mol^{-1} lower than the barrier for TS1, indicating that water may act as an effective catalyst. However, as the energy required for reaction is still significantly higher than the energy required to break apart the complex, it is unlikely that this route will be important unless the presence of further molecules (i.e., solvent) would act to trap the reacting complex. The corresponding G2 value in the $H_2O{\cdot}H_2O{\cdot}SO_2$ system[11] is a barrier of 84 kJ mol^{-1}, lowered 58 kJ mol^{-1} by the presence of the second water molecule.

Though the intermediate (I) in all its forms may form a van der Waals complex with water, only the VdW5 complex between water and (I)b was studied. Water was found to bind with (I)b with an energy in the range of 13 (CCSD(T) with full counterpoise) to 19 (G3) kJ mol^{-1}. The resulting complex can then undergo a similar molecular rearrangement to the previous step to form S_2O and two water molecules. The barrier for this process is 86 kJ mol^{-1}, a lowering of 35 kJ mol^{-1} relative to the uncatalyzed reaction. Again, significantly more energy is required to overcome this barrier than to break apart the complex.

The kinetic treatment of this series of reactions was designed to describe the most important contribution of the possible elementary reactions between species to understand what conditions are required for the catalysis by water. The reaction between H_2O and SO_2 to form VdW1 was assumed to be barrierless and to occur at the same rate as collision. This describes rapid equilibrium that is predominantly shifted to the reactant side due to entropic considerations. The reaction between VdW1 and H_2S could be treated in the same manner to describe the formation of VdW4; however, it is unlikely that this complex would be stable under combustion conditions due to its weak nature. Instead, the reaction between VdW1 and H_2S to form (I) + H_2O can be treated as a bimolecular reaction with a barrier of 73 kJ mol^{-1}, substantially lower than the barrier to the direct reaction of dry $H_2S + SO_2$. In a similar manner, the reaction between (I) and H_2O can be treated as a bimolecular reaction producing $S_2O + 2H_2O$, with a barrier of 68 kJ mol^{-1}.

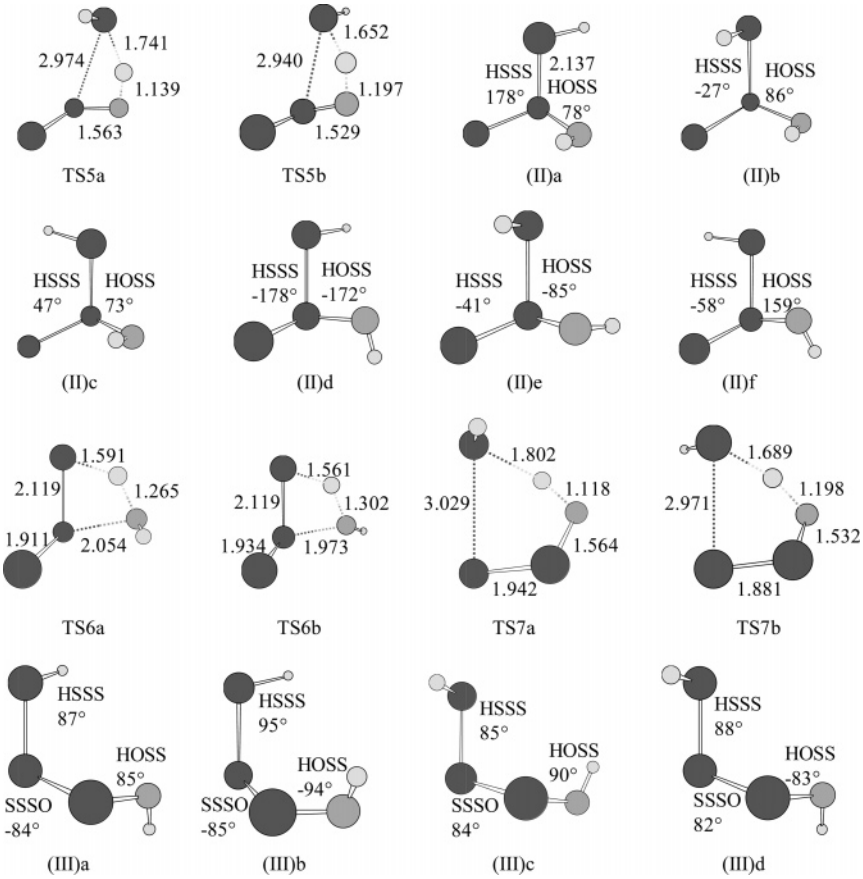

Figure 6. Molecular geometries of the species on the H_2S_3O potential energy surfaces. Bond lengths in Å.

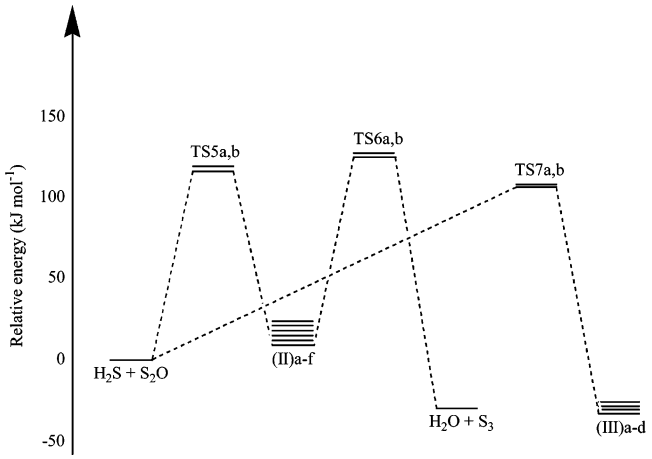

Figure 7. Potential energy surface for the reaction between H_2S and S_2O.

Although the barrier for reaction between H_2S and SO_2 is ~60 kJ mol^{-1} lower when the SO_2 is complexed with H_2O (i.e., VdW1), under combustion conditions the negligible amount of VdW1 renders this reaction relatively unimportant. The nature of TS3, however, does provide insight into the first step of the aqueous Wackenroder reaction,[21] with further complexation and solvation effects likely to reduce the barrier to reaction further and provide an environment where H_2O can act as an effective catalyst.

H_2S_3O Surface. S_2O, an analogue of SO_2, can react with H_2S to ultimately produce H_2O + S_3. The reaction follows a mechanism similar to that for reaction between H_2S and SO_2 and the transition states and intermediates were dealt with in the same manner as described earlier. The initial barrier for the reaction (TS5a,b) is ~115 kJ mol^{-1}, 20 kJ mol^{-1} lower in energy than the corresponding barrier on the $H_2S_2O_2$ surface. The intermediate formed, (II), has a number of rotamers, the lowest of which is just 8 kJ mol^{-1} above the reactants, ~20 kJ mol^{-1} more stable than on the $H_2S_2O_2$ surface. The barrier to forming products via TS6a,b is 116 kJ mol^{-1}, only slightly lower than on the $H_2S_2O_2$ surface. Overall, the reaction is 31 kJ mol^{-1} exothermic versus 16 kJ mol^{-1} endothermic for the reaction between H_2S and SO_2.

TABLE 3: Relative Energies of Species on the H_2S_3O Potential Energy Surface

	relative energy (kJ mol^{-1})		
species	G2	G3	lit. values
$H_2S + S_2O$	0	0	0
TS5a	120[a]	117[a]	
TS5b	119[a]	115[a]	
(II)a	13	8	
(II)b	16[b]	11[b]	
(II)c	17[b]	13[b]	
(II)d	26[b]	22[b]	
(II)e	26[b]	22[b]	
(II)f	27[b]	23[b]	
TS6a	126[a]	124[a]	
TS6b	127[a]	127[a]	
$S_3 + H_2O$	−32	−31	−27[d]
TS7a	113[a]	109[a]	
TS7b	113[c]	107[c]	
(III)a	−34	−35	
(III)b	−33[b]	−35[b]	
(III)c	−33[b]	−35[b]	
(III)d	−32[b]	−34[b]	

[a] CASSCF(6,6)/6-31G(*d*) optimized geometry. [b] Energies relative to (II)a and (III)a, respectively, calculated at the G2 and G3 levels with MP2/6-31G(*d*) frequencies. [c] HF/6-31G(*d*) geometry. [d] 298 K values calculated from $\Delta H^0_{f,298}$ from NIST webbook[26] and from ref 27.

TABLE 4: Kinetic Parameters for Reaction Scheme

reaction	*A* factor[a]	*n*	E_a[b]	
R1	$H_2S + SO_2 \rightarrow$ (I)[c]	3.51×10^{18}	−2.121	140
R2	$H_2S + SO_2 \rightarrow H_2O + S_2O$[c]	1.67×10^{6}	1.857	158
R1 + R2	$H_2S + SO_2 \rightarrow$ products [c]	2.21×10^{12}	−0.187	132
R3	$H_2O + SO_2 \rightarrow$ VdW1	$\sim 10^{14}$	0	0
R4	VdW1 + $H_2S \rightarrow$ (I) + H_2O	7.70×10^{-1}	2.449	55
R5	(I) + $H_2O \rightarrow 2H_2O + S_2O$	3.64×10^{5}	1.562	60
R6	$H_2S + S_2O \rightarrow$ (II)[c]	2.38×10^{19}	−2.307	127
R7	$H_2S + S_2O \rightarrow H_2O + S_3$[c]	8.01×10^{7}	1.506	142
R8	$H_2S + S_2O \rightarrow$ (III)[d]	2.85×10^{0}	3.638	95

[a] Units s^{-1} for unimolecular reactions, $cm^3\ mol^{-1}\ s^{-1}$ for bimolecular reactions. [b] Units kJ mol^{-1}. [c] Calculated using QRRK in 1 atm N_2. [d] High-pressure limit.

TABLE 5: Thermodynamic Parameters for Intermediates and Complexes

property	*T* (K)	S_2O[a]	(I)[b]	VdW1[c]	(II)[b]	(III)[b]
$\Delta_f H^0$ (kJ mol^{-1})	298	−57.6	−291.8	−549.2	−74.7	−117.3
S (J K^{-1} mol^{-1})	298	266.4	325.6	346.8	337.1	343.7
C_p (J K^{-1} mol^{-1})	298	43.8	83.0	86.2	92.7	86.9
	300	43.8	83.3	86.3	93.0	87.1
	400	47.4	95.2	91.4	101.8	96.4
	500	50.0	103.4	95.8	107.6	102.6
	600	51.9	108.7	99.7	111.4	107.1
	700	53.2	112.3	102.9	114.1	110.5
	800	54.2	114.9	105.6	116.2	113.2
	900	54.9	117.0	108.0	118.0	115.5
	1000	55.5	118.6	110.1	119.5	117.4
	1100	55.9	120.1	112.0	120.8	119.1
	1200	56.2	121.3	113.7	122.0	120.5
	1300	56.5	122.4	115.3	123.0	121.8
	1400	56.7	123.3	116.7	124.0	122.9
	1500	56.9	124.2	118.0	124.8	123.8
	1600	57.1	124.9	119.2	125.5	124.7
	1700	57.2	125.6	120.3	126.1	125.4
	1800	57.3	126.2	121.2	126.7	126.1
	1900	57.4	126.7	122.1	127.2	126.6
	2000	57.5	127.2	122.9	127.7	127.2

[a] Thermodynamic properties based on the G3 method. [b] Thermodynamic properties based on the G3 method with inclusion of rotamers and optical isomers in the partition function. [c] Thermodynamic properties based on MP2(full)/6-311++G(d,p) geometries and scaled vibrational and counterpoise-corrected CCSD(T)/6-311++G(d,p) energies.

A QRRK analysis of this reaction was carried out at atmospheric pressure, with the boiling point of (II) chosen to be 540 K, 30 K higher than the boiling point of H_2S_4. At 2000 K, ~11% of reaction flux over TS5 continued over TS6 to produce $H_2O + S_3$, at 300 K this was ~0.002%. At 300 K >99% of reaction flux over TS5 was stabilized as (II), whereas by 2000 K this had decreased to ~2%.

H_2S and S_2O can also react via a five-membered ring (TS7a,b) to produce a linear species (III), analogous to H_2S_4. The barrier to this reaction is 107 kJ mol^{-1}, slightly lower than the reaction to produce (II). As no CASSCF geometry could be located for TS7b, the SCF geometry was used as in normal G2 and G3 theory. The linear species has four distinct rotamers, as well as optical isomerism, with the most stable form (III)a being 35 kJ mol^{-1} lower in energy than $H_2S + S_2O$. The corresponding linear species on the $H_2S_2O_2$ surface, (HSSOOH) was found to be more than 200 kJ mol^{-1} higher in energy than (I) and was thus not considered further.

Given the low barrier of the self-reaction of S_2O,[7] the two pathways reported here would occur only when $[H_2S] \gg [S_2O]$.

3.2. Comparison with Experimental Observations of the Claus Reaction. There have been a number of studies of the reaction of H_2S with SO_2, but the results are generally found to be affected by catalytic effects at the reactor walls,[22,23] especially at lower temperatures. Tesner[22] attempted to separate out the homogeneous component of the reaction rate and reported an apparent activation energy of 60 kJ mol^{-1} for the overall reaction to produce sulfur vapor. At 960 K, the lowest temperature of Tesner's experiments, his nominally homogeneous rates are many orders of magnitude greater than our expression for reaction of $H_2S + SO_2$ (Table 4, reaction R2) would predict. However at Tesner's highest temperatures, his rates are nearer to those corresponding to R2, which has a much higher activation energy than he found (158 kJ mol^{-1} vs 60 kJ mol^{-1}). It is suspected that Tesner's results at lower temperature may well be affected by heterogeneous reactions.

Monnery et al.[24] studied the reaction under dilute conditions (1.13% SO_2 with 1.96% H_2S) in a flow reactor at atmospheric pressure, for temperatures from 1123 to 1423 K. They measured the loss of reactant as a function of residence time and showed their results to be free of surface catalysis. They fitted their results for the kinetics of the overall reaction $H_2S + {}^1/_2SO_2 \rightarrow {}^3/_4S_2 + H_2O$ to a global kinetic expression with an activation energy of 209 kJ mol^{-1}. This value is now significantly larger than the 158 kJ mol^{-1} found in the present work for the production of H_2O from $H_2S + SO_2$ via R2. At the maximum temperature of 1423 K studied by Monnery et al., the initial rate of disappearance of H_2S predicted from their global expression is a factor of 25 higher than our result for R2. This factor rises to 75 at their lowest experimental temperature of 1123 K.

The high value for the global activation energy reported by Monnery et al.[24] suggests that their results are not unduly affected by surface catalysis of the direct reaction between H_2S and SO_2. However, their experimental rate is much greater than our results could explain, despite the fact that the theoretical activation energy is significantly lower than they reported. It was noted[24] that the temperatures of their study are high enough for the thermolysis of H_2S itself to be a significant route to H_2S decomposition, even without SO_2, and the question arises as to whether there are not interactions between the H_2S thermolysis process and the apparent progress of the overall Claus reaction.

We have previously developed a detailed mechanism for the thermolysis of H_2S.[4] In validating this mechanism, we were able to fit the data of Hawboldt et al.[25] for H_2S thermolysis in the absence of SO_2, obtained in the same reactor as the data for the Claus reaction.[24] Our model shows that 70% of the H_2S in the Claus experiments would be expected to decompose even in the absence of SO_2 and therefore that the 87% decomposition observed experimentally cannot be ascribed solely to a "Claus" process. Of course, the decomposition of SO_2 found under Claus conditions cannot be explained by our thermolysis model, but the implication is that SO_2 decomposition in these experiments does not come solely from direct reaction of SO_2 with H_2S, but rather also involves interaction of SO_2 with the thermolysis intermediates (H, S, HS, S_2, HSS, HSSH, and H_2). Depletion of (I) via reaction of thermolysis intermediates could also occur under these conditions. A preliminary examination of the kinetics of reaction of SO_2 under H_2S thermolysis conditions has been undertaken using a published mechanism for the behavior of SO_2 in fuel-rich combustion conditions.[3] Negligible extents of SO_2 reaction are predicted except via the direct Claus reaction (R2) and the experimental results remain unexplained.

In the front-end Claus reactor, H_2S is combusted with one-third of the stoichiometric requirement of O_2, to produce the ratio of H_2S:SO_2 = 2:1 needed for optimal performance of the downstream catalytic Claus reactors. However, the actual

conversion of H_2S can be over 60%, and this has been attributed to the occurrence of the homogeneous Claus reaction (R2).[24] However, a kinetic model (ref 3 plus H_2 combustion chemistry) of the typical reaction conditions encountered in the front-end furnace of the modified Claus process suggests that much of the excess reaction may be attributed to other processes. Thus, for inlet concentrations $x_{H_2S} = 30\%$, $x_{O_2} = 15\%$, $x_{N_2} = 55\%$ at 1 bar and 1500 K, the model predicts about 70% conversion of H_2S without including R2. The excess consumption of H_2S is thermolytic, yielding S_2 and H_2. Some oxygen is consumed in oxidizing H_2 and the yield of SO_2 is therefore less than expected, more or less as would be found if the gas-phase Claus process had been a significant reaction. Thus, much of what has been attributed to the gas-phase Claus process may actually be a combination of H_2S oxidation and pyrolysis.

4. Conclusions

The direct reaction between H_2S and SO_2, studied at the G2 and G3 levels of theory, results in the formation of thiosulfurous acid HSS(O)OH, with a barrier of approximately 135 ± 15 kJ mol^{-1}, the precise height of the barrier depending on the method (± 3 kJ mol mol^{-1}), and on the specific isomers in the transition state (± 2 kJ mol^{-1}). The thiosulfurous acid itself can rearrange and dissociate to yield S_2O and H_2O, with a barrier of approximately 120 kJ mol^{-1}, which is higher than the barrier for decomposition back to reactants (105 kJ mol^{-1}). On the basis of QRRK analysis, the kinetics of the overall reaction to produce $H_2S + SO_2 \rightarrow S_2O + H_2O$ at atmospheric pressure may be represented as $k = 1.67 \times 10^6 T^{1.85} \exp(-158 \text{ kJ mol}^{-1}/RT)$ cm^3 mol^{-1} s^{-1}.

Both the reaction to form thiosulfurous acid and the decomposition of the acid to form $S_2O + H_2O$ are catalyzed by water through the formation of van der Waals complexes. However, because of the weak nature of the intermediate complexes, these reactions would not be expected to play a significant part in the overall reaction at atmospheric pressure.

The S_2O produced in the overall reaction between H_2S and SO_2 is both an analogue of SO_2 and a potential reactant with H_2S. Although the reaction $H_2S + S_2O \rightarrow H_2O + S_3$ displays reaction pathways and energies that are precisely analogous to those for $H_2S + SO_2$, there is now a second addition and rearrangement channel, to form HOSSSH, that is available with lower activation energy (95 kJ mol^{-1}).

The good agreement between the G2 and G3 results indicates that repeating previous studies [4,11] at the more recent level of theory is unlikely to alter the predictions of such models.

The predicted rate of the overall direct Claus reaction R2 is insufficient to account for experimental observations in flow reactors. On the other hand, the apparent extent of interaction between H_2S and SO_2 in the front-end furnace of the modified Claus process may be qualitatively accounted for through the simultaneous thermolysis and oxidation of H_2S. Further work is needed to provide data free of surface effects and to develop more comprehensive chemical kinetic models of H_2S oxidation.

Acknowledgment. The work has been funded by the Australian Research Council and by the University of Sydney through the HB and FM Gritton Bequest.

Supporting Information Available: Geometries and vibrational frequencies of all species presented. This material is available free of charge via the Internet at http://pubs.acs.org.

References and Notes

(1) Glarborg, P.; Kubel, D.; Dam-Johansen, K.; Chiang, H.-M.; Bozzelli, J. W. *Int. J. Chem. Kinet.*, **1996**, *28*, 773−790.
(2) Alzueta, M. U.; Bilbao, R.; Glarborg, P. *Combust. Flame* **2001**, *127*, 2234−2251.
(3) Leeds University Sulphur Mechanism, version 5.2; http://www.chem.leeds.ac.uk/Combustion/sox.htm/.
(4) Sendt, K.; Jazbec, M.; Haynes, B. S. *Proc. Combust. Inst.* **2002**, *29*, 2439−2446.
(5) Miaskiewicz, K.; Steudel. R. *J. Chem. Soc., Dalton Trans.* **1991**, 2395−2399.
(6) Drozdova, Y.; Steudel, R. *Chem. Eur. J.* **1995**, *1*, 193−198.
(7) Steudal, R.; Steudal, Y. *Eur. J. Inorg. Chem.* **2004**, *17*, 3513−3521.
(8) Curtiss, L. A.; Raghavachari, K.; Trucks G. W.; Pople, J. A. *J. Chem. Phys.* **1991**, *94*, 7221−7230.
(9) Curtiss, L. A.; Raghavachari, K.; Redfern, P. C.; Rassolov, V.; Pople, J. A. *J. Chem. Phys.* **1998**, *109*, 7764−7776.
(10) Scott, A. P.; Radom, L. *J. Phys. Chem.* **1996**, *100*, 16502−16513.
(11) Li, W.-K.; McKee, M. L. *J. Phys. Chem A* **1997**, *101*, 9778−9782.
(12) van Duijneveldt, F. B. Basis Set Superposition Error. In *Molecular Interactions From van der Waals to Strongly Bound Complexes*; Scheiner, Steve, Ed.; John Wiley and Sons: New York, 1997; pp 81−104 .
(13) Frisch, M. J.; Trucks, G. W.; Schlegel, H. B.; Scuseria, G. E.; Robb, M. A.; Cheeseman, J. R.; Zakrzewski, V. G.; Montgomery, J. A., Jr.; Stratmann, R. E.; Burant, J. C.; Dapprich, S.; Millam, J. M.; Daniels, A. D.; Kudin, K. N.; Strain, M. C.; Farkas, O.; Tomasi, J.; Barone, V.; Cossi, M.; Cammi, R.; Mennucci, B.; Pomelli, C.; Adamo, C.; Clifford, S.; Ochterski, J.; Petersson, G. A.; Ayala, P. Y.; Cui, Q.; Morokuma, K.; Malick, D. K.; Rabuck, A. D.; Raghavachari, K.; Foresman, J. B.; Cioslowski, J.; Ortiz, J. V.; Stefanov, B. B.; Liu, G.; Liashenko, A.; Piskorz, P.; Komaromi, I.; Gomperts, R.; Martin, R. L.; Fox, D. J.; Keith, T.; Al-Laham, M. A.; Peng, C. Y.; Nanayakkara, A.; Gonzalez, C.; Challacombe, M.; Gill, P. M. W.; Johnson, B. G.; Chen, W.; Wong, M. W.; Andres, J. L.; Head-Gordon, M.; Replogle, E. S.; Pople, J. A. *Gaussian 98*, revision A; Gaussian, Inc.: Pittsburgh, PA, 1998.
(14) Helgaker, T.; et al. *Dalton release 1.1 2000, an electronic structure program*.
(15) McQuarrie, D. A. *Statistical Mechanics*; Harper and Row: New York, 1976.
(16) Steinfeld, J. I.; Fransisco, J. S.; Hase, W. L. *Chemical Kinetics and Dynamics*; Prentice Hall: Englewood Cliffs, NJ, 1989.
(17) Wigner, E. *Z. Phys. Chem. B* **1932**, *19*, 203−216.
(18) Garrett, B. C.; Truhlar, D. G. *J. Phys. Chem.* **1979**, *83*, 200−203.
(19) Dean, A. M. *J. Phys. Chem.* **1985**, *89*, 4600−4608.
(20) Bishenden, E.; Donaldson, D. J. *J. Phys. Chem. A* **1998**, *102*, 4638−4642.
(21) Schenk, P. W.; Steudel, R. *Angew. Chem. Int. Ed.* **1965**, *4*, 402−409.
(22) Tesner, P. A.; Nemirovskii, M. S.; Motyl, D. N. *Kinet. Catal.* **1990**, *30*, 889−892.
(23) Loura, B. B.; Olga, F. *J. Chim. Phys.* **1996**, *93*, 1364−1375.
(24) Monnery, W. D.; Hawboldt, K. A.; Pollock, A.; Svrcek, W. Y. *Chem. Eng. Sci.* **2000**, *55*, 5141−5148.
(25) Hawboldt, K. A.; Monnery, W. D.; Svrcek, W. Y. *Chem. Eng. Sci.* **2000**, *55*, 957−966.
(26) Chase, M. W. J. NIST-JANAF Thermochemical Tables, 4th ed. *J. Phys. Chem. Ref. Data* **1998**, Monograph 9.
(27) Steudel, R. *Top. Curr. Chem.* **2003**, *230*, 117−134.